A Robust Smart Window: Reversibly Switching from High Transparency to Angle-Independent Structural Color Display

*Dengteng Ge, Elaine Lee, Lili Yang, Yigil Cho, Min Li, Daniel S. Gianola, and Shu Yang**

Commercial buildings in the United States alone account for nearly 40% of the total energy consumption. Among them, electricity is the largest energy source for buildings. Therefore, the design of new energy efficient materials and technologies is crucial to meet goals such as the Net-Zero Energy Commercial Building Initiative (CBI) put forward by the U.S. Department of Energy (DOE). There has been tremendous interest in economizing energy uses in buildings through house roofing, skylights, and architectural windows.[1–3] For example, smart windows have been developed, which become opaque to block or reflect sunlight on scorching days to save air conditioning costs, and return to a transparent state at a low lighting condition to improve light harvesting and capture free heat from the sun.[1,4–6] Typically, optical-modulation in window or coating materials is realized through an external stimuli-triggered switch in chemistry and/or morphology to produce a change in optical properties, including the use of suspended particles,[7] polymer dispersed liquid crystals (PDLCs),[8–12] and chromogenic materials driven by ion and electron insertion/extraction, light,[5] temperature,[13] and electrical field.[14] The assembly of the device is often complex, and many of the components are chemically unstable and costly. Therefore, facile material handling and fabrication is desirable for large-area smart windows with switchable optical properties.

Structural color resulting from the interference, diffraction, and scattering of light from micro- or nanostructures with feature size on the order of the wavelength of light[15–17] offers a promising alternative to dynamically tune the optical properties of materials in response to external stimuli without changing their bulk properties.[15–17] In nature, bio-organisms switch color/opaqueness and/or transparency to suit the local environment for hiding from their predators, for signaling, or for mating purposes.[18–21] For example, squids and octopuses in the deep sea are masters of disguise. They are normally transparent in sea, thus invisible to a predatory fish in downwelling light. They can quickly turn into red, however, thus becoming invisible again to fish with bioluminescent searchlights.[22] They alternate their body color by stretching the skin to enlarge the embedded chromophores.[23]

Mechanical modulation is a common practice to control light transmission macroscopically, such as the opening and closing of curtains and blinds. However, mechanical driving of macroscopic units is cumbersome and they must communicate through a mainframe. It is highly desirable to develop a skin-like material/device that can be integrated into building components to change transparency or color. At the micro- and nanoscales, tuning of the optical properties by mechanical stretching and compressing has been demonstrated from patterned polymer thin films, including micro-[24] and nanopillar arrays[25] on wrinkled poly(dimethylsiloxane) (PDMS), shape memory polymers consisting of periodic microhole arrays[26] and micro-optic components.[27] Many of them have inherent, angle-dependent structural color due to Bragg diffraction from the periodic structures. Typically, the initial state is opaque or colored, attributed to the pre-existing micro-/nanostructures. The windows exhibit increased transmission upon stretching due to the reduction of surface roughness, thus less scattering. However, the roughness of the materials and the resulting light scattering cannot be completely eliminated. Therefore, it is difficult to achieve high transparency with >90% transmittance in the visible region either before or after mechanical modulation.

Here, we prepared a composite film consisting of a thin layer of quasi-amorphous array of silica nanoparticles (NPs) embedded in bulk elastomeric PDMS. Importantly, it was highly transparent (>90% transmittance in the visible wavelength) in the initial state. Upon mechanical stretching, the transmittance was dramatically reduced to 30% and displayed angle-independent structural color at a strain >40%. The color could be tuned by the silica NP size. Unlike the silica NPs/PDMS films prepared from highly ordered silica colloidal crystals,[28] the reflective color was invariant with increased strain. The switch between transparency and colored states could be reversibly cycled at least 1000 times without losing the film's structural and optical integrity.

The fabrication of the smart window is illustrated in **Figure 1**a. First, the silica NP solution was spray-coated onto a polystyrene substrate following the procedure reported earlier to create superhydrophobic, angle-independent color coatings from quasi-amorphous NP arrays.[29] Here, angle-independent blue, green, and pink films (Figure 1b) were obtained from silica NPs with diameters of 221, 258, and 306 nm, respectively. As shown in scanning electron microscopy (SEM) images, the particles formed quasi-amorphous arrays with short-range ordering yet were long-range disordered (Figure 1c), in agreement with our prior observation.[29] PDMS precursor solution was then cast

Dr. D. Ge, E. Lee, Dr. Y. Cho, M. Li, Prof. D. S. Gianola, Prof. S. Yang
Department of Materials Science and Engineering
University of Pennsylvania
3231 Walnut Street
Philadelphia, PA 19104, USA
E-mail: shuyang@seas.upenn.edu
Prof. L. Yang
School of Transportation Science and Engineering
Harbin Institute of Technology
Harbin 150090, PR China

DOI: 10.1002/adma.201500281

ADVANCED MATERIALS
www.advmat.de

Materials Views
www.MaterialsViews.com

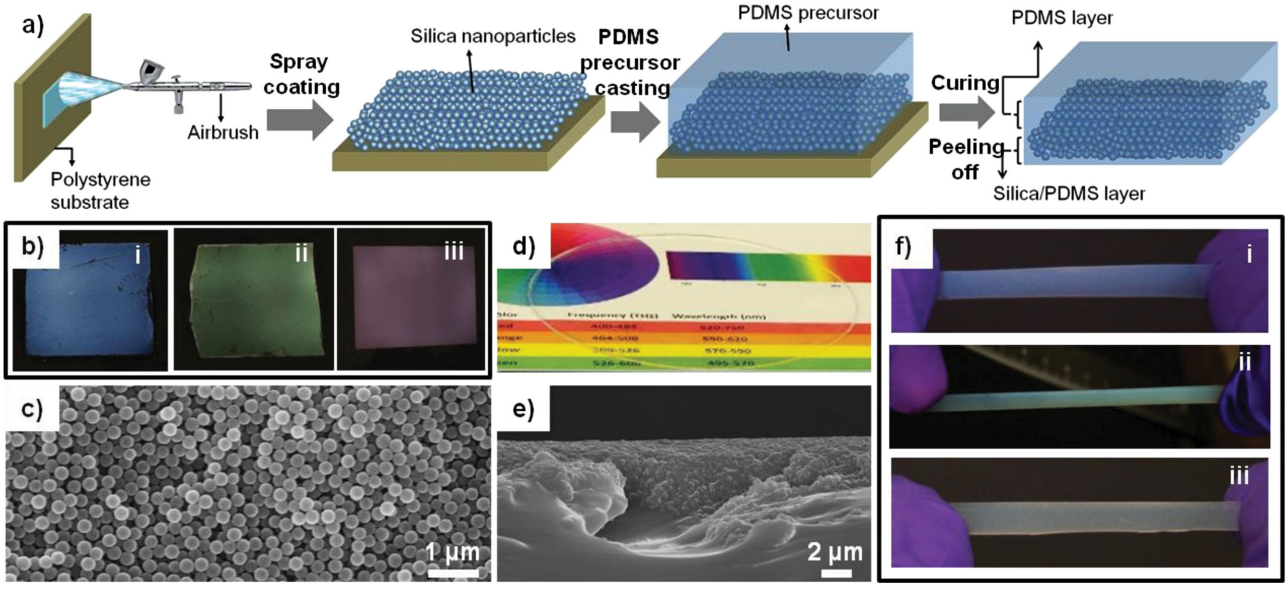

Figure 1. a) Schematic of the smart window fabrication process. b) Digital photographs of the nanoparticle films prepared with nanoparticles of diameter: i) 221, ii) 258, and iii) 306 nm. c) SEM image of nanoparticle film showing quasi-amorphous ordering. d) Digital photograph and e) SEM image of the highly transparent silica/PDMS composite film. f) Digital photographs of stretched silica/PDMS films with embedded nanoparticles of diameter: i) 221, ii) 258, and iii) 306 nm, respectively.

over the NP film, filling the voids between the particles. Since the refractive index of PDMS (1.425 at 632.8 nm)[30] is very close to that of silica (1.457 at 632.8 nm),[31] the composite films were highly transparent in the visible and near infrared (vis–NIR) range, as seen in Figure 1d. Indeed, it is difficult to discern the PDMS films with and without embedded silica NPs.

Under SEM, it could be seen that the films had two layers: a thin layer of hard silica NP/PDMS composite (4–5 μm thick) and a bulk layer of pure PDMS (Figure 1e). The thickness of the pure PDMS layer ranged from 0.5 to 1 mm depending on the amount of PDMS solution used in casting. Close-packed silica NP films were also prepared for comparison. The latter tended to rupture easily at the interface between the composite layer and the pure PDMS layer when peeled off from the supporting substrate due to the narrow PDMS ligaments (<20 nm)[32] between the close-packed silica NPs. In comparison, the quasi-amorphous structure of spray-coated NP films possessed rather random, thus larger, pores from place to place to infiltrate PDMS. The resulting thicker PDMS layers between the silica NPs offered much higher mechanical strength against macroscopic rupture. Upon stretching, two optical phenomena were observed: i) switching from transparency to opacity (Video S1, Supporting Information), and ii) appearance of uniform, angle-independent reflective color, blue, green, and yellow–white from the films with silica NPs of diameter 221, 258, and 306 nm, respectively (Figure 1f). These phenomena are reversible upon release of the strains.

To investigate the origin of these phenomena, which have not been reported in the literature, we used optical microscopy and SEM to monitor the silica NP/PDMS films stretched at various strains (**Figure 2**a,b). As seen with optical microscopy in reflectance mode (Figure 2a), microcracks began to appear (Figure 2a-ii) when the strain level reached 20%. With further increase of strain, the number and length of microcracks increased and wrinkling began to occur transverse to the applied strain with wavelength of ≈25 μm (Figure 2a-iii). The wrinkle formation can be explained by the mismatch of mechanical properties of the bilayer structure of the silica NP/PDMS composite film.[33] In addition, the optical images taken in reflection mode showed that color appeared randomly in the film. Since the inside of the composite layer could not be imaged clearly under reflection mode, transmission mode was used to image the film instead (Figure 2b). Figure 2b-iii,b-iv showed that the whole film was yellow/purpleish, complementary to the reflective color of blue and green seen in Figure 1f-ii under transmission mode. However, surface wrinkles and microcracks are not the only reasons contributing to the displayed color. Nanosized voids were also observed from the cross-sectional SEM of the composite film under ≈40% strain (Figure 2c), and PDMS ligaments between the particles were highly stretched, while the silica NPs remained embedded. Voids tended to form locally in high stress regions, rather than across the whole film. To better image the in-plane structure of the composite film and the formation of the voids under mechanical strain, we fabricated a PDMS film dispersed with silica particles of larger diameter, 5 μm, and imaged the film before and after stretching using confocal microscopy. As seen in Figure 2d, microvoids were formed on both sides of the silica microparticles parallel to the stretching direction. It is known that PDMS can detach easily from the silica particles because of the low adhesion force (≈10 kPa) between PDMS (hydrophobic) and untreated silica (hydrophilic).[34,35] When the strain is released, the voids are closed and this process can be reversibly repeated.

With knowledge of the film morphology under various strains, the transmittance of the film was investigated using UV–vis–NIR spectroscopy. By naked eyes, the transparent, as-prepared silica NP/PDMS film began to look translucent at about 20% strain and was completely opaque at about 100%

Adv. Mater. **2015**,
DOI: 10.1002/adma.201500281

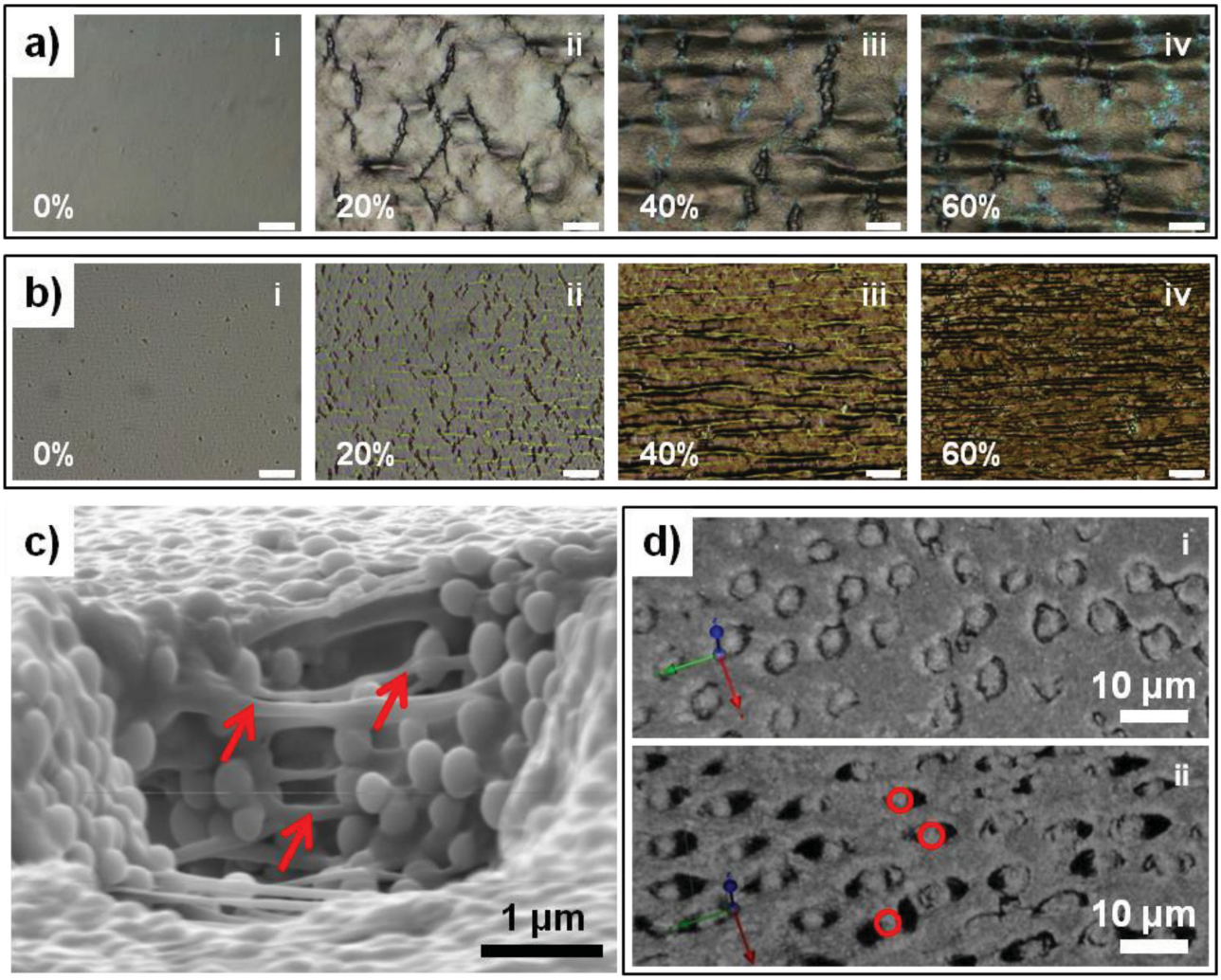

Figure 2. Optical images of a silica/PDMS film consisting of nanoparticles of diameter 258 nm at various strains in a) reflection and b) transmission modes (Scale bars: 20 μm). c) SEM image of a stretched silica/PDMS film with nanoparticles of diameter 258 nm at ≈80% strain. Arrows indicate PDMS ligaments. d) Confocal optical image of an unstretched (i) and a stretched (ii) silica nanoparticle (diameter of 5 μm)/PDMS film. The circles indicate silica nanoparticles. Black regions indicate the voids.

strain (**Figure 3**a). The strain–transmittance curves (Figure 3b) showed three stages, corresponding to wrinkle and crack formation at 0–20% strain level, void formation at 20–80% strain level, and leveling-off at >80% strain, in agreement with observation from optical microscopy shown in Figure 2a,b. The transmittance decreased the most at the void formation stage, suggesting that void formation was mainly responsible for the transparency change in our smart window. The transmittance is dependent on the size of the silica NPs and thus, the resulting voids from mechanical strain (see Figure S1, Supporting Information). Smaller particles (221 nm in diameter) and voids have low transmittance at shorter wavelengths due to Rayleigh scattering, which is wavelength-dependent. Larger particles (258 and 306 nm in diameters) and voids mainly have Mie scattering, which is wavelength-independent. The average transmittance in the visible wavelength range (400–700 nm) of the as-prepared silica NP/PDMS film and a pure PDMS film were measured to be ≈92% and ≈94%, respectively (Figure 3c). When stretched, a significantly large drop in the transmittance of the silica NP/PDMS film in the visible region was observed (Figure 3c and Figure S1, Supporting Information): over 50% in average for different particle sizes and the largest change was nearly 70%, much higher than those reported in literature.[24,25]

To demonstrate repeatability and robustness of our smart window, we stretched and released the films from 20% to 70% strain at a frequency of 0.5 Hz for 1000 times, and the transparency was measured continuously at 500 nm. The transmittance of the films after stretching and releasing 1000 times was nearly identical to that of the unstretched film (see Figure 3b inset). We believe that the durability and stability of the films can be attributed to the combination of thick PDMS layer (0.5–1 mm) and thin silica NP/PDMS composite layer (≈4–5 μm). While the top thin layer is responsible for color/transmittance change, the bottom thick PDMS layer produces necessary restoring force for the entire film for repeated stretching and release. Meanwhile, the elastic PDMS nanoscale ligaments generated during stretching in the composite layer (see Figure 2c) played a role to confine the silica NPs in their local regions, where color

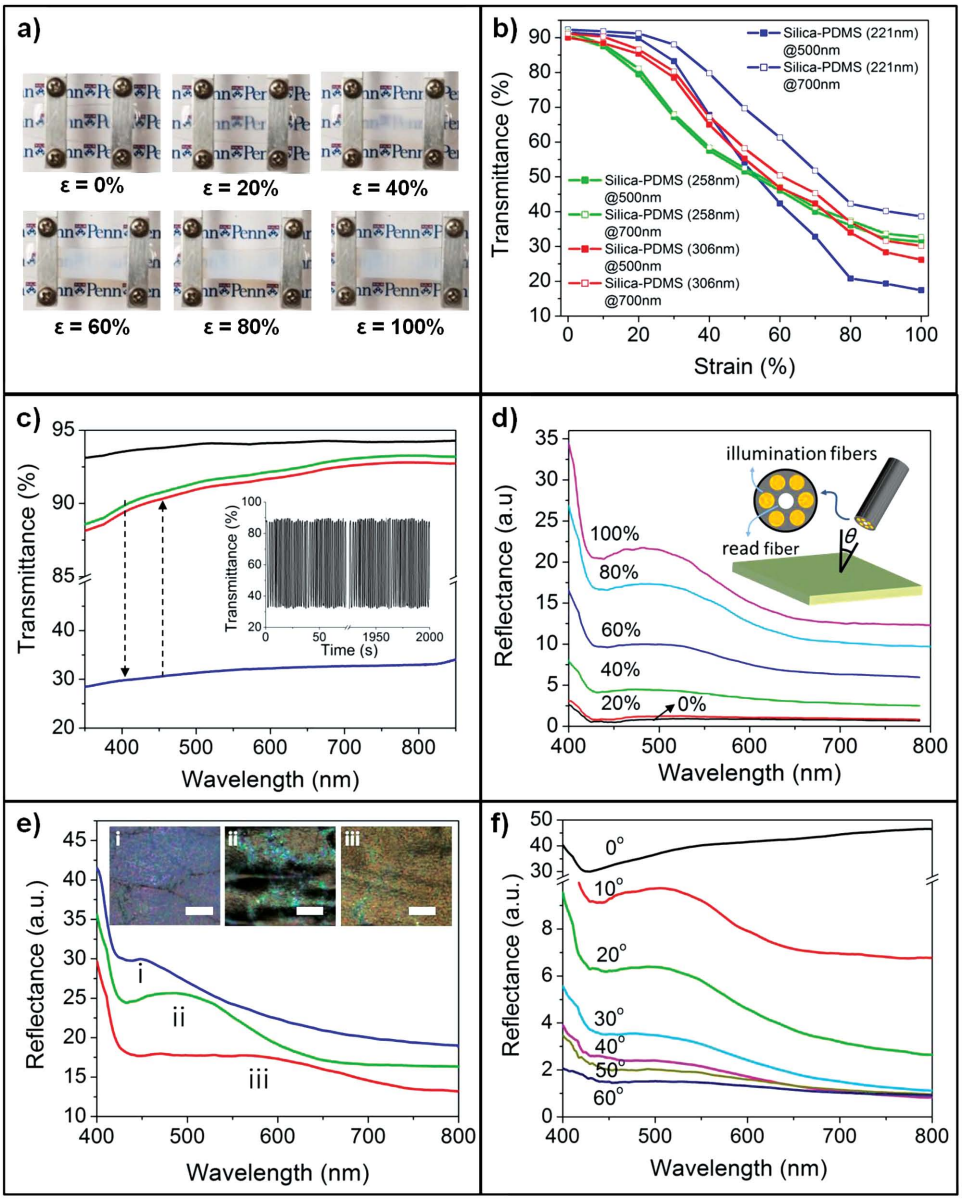

Figure 3. a) Digital photographs of a silica/PDMS film consisting of nanoparticles of diameter 258 nm at various strains. b) Transmittance spectra of a pure PDMS film (black), an as-prepared silica nanoparticle/PDMS film (green), and a silica nanoparticle/PDMS film stretched at 100% strain (blue) and released (red) 1000 times. Inset: Transmittance change as a function of stretching/release cycles. c) Transmittance versus strain at wavelengths of 500 and 700 nm, respectively. d) Reflectance spectra of the composite film with nanoparticle diameter of 258 nm at various strains at a viewing angle of 10°. Inset: schematic illustration of the viewing angle in the experimental setup. e) Reflectance spectra of silica nanoparticle/PDMS films with 80% strain at a viewing angle of 10°. The nanoparticles have diameters of: i) 221, ii) 258, and iii) 306 nm, respectively. Inset: optical images of the stretched silica/PDMS membrane with nanoparticles of diameter of: i) 221, ii) 258, and iii) 306 nm, respectively. Scale bars: 20 μm. f) Reflectance spectra of the composite film with nanoparticle diameter of 258 nm with 80% strain at various viewing angles.

appeared and intensified upon stretching but did not change for a given NP size.

To characterize the color of the smart windows, we measured the reflectance of the films at different strain levels in the vis–NIR range using a custom-built spectrophotometer outfitted with a reflectance and backscattering optical fiber (Ocean Optics), as shown in Figure 3d inset. Reflectance peaks started to appear at 40% strain and intensified at strains >60% (Figure 3d), which matched the formation of microwrinkles and nanovoids shown in Figure 2. The peak position did not noticeably change with increase of strain. We note that the color of quasi-amorphous silica NP array (Figure 1b and Figure S2, Supporting Information), however, is different from that of silica NP/PDMS film (Figures 1f and 3e) of the same NP size. As seen in Figure S2, Supporting Information, the reflectance peaks (λ_R) of the silica NP arrays were dependent on the size of NPs, in agreement with literature:[36,37] blue (NP diameter, 221 nm), green (258 nm), and pink (306 nm) films had reflectance

Adv. Mater. 2015,
DOI: 10.1002/adma.201500281

peaks at 461, 517, and 625 nm, respectively. At 80% strain and a viewing angle of 10°, the reflectance peaks of the films prepared with 221, 258, and 306 nm silica NPs were at wavelengths 454, 501, and 587 nm, respectively (Figure 3e). The reflectance peaks of the stretched silica NP/PDMS films were blue-shifted compared to pure NP films of the same NP size, but there was no further change of peak position at various strains. We then tilted the films with respect to the detector. As seen in Figure 3f, the reflectance peak positions did not change with the viewing angles, characteristic of quasi-amorphous structural color. Instead, the reflectance peak intensity is dependent on the viewing angle and maximized at a viewing angle of 10°. In contrast, optically switchable windows reported in literature typically produce angle-dependent color due to Bragg diffraction of the highly ordered structures.[24,27]

Based on our observations and measurements, we proposed a mechanism of void formation in **Figure 4**a, where the changes in the optical properties could be attributed to the microstructural change, including microroughness from wrinkles and nanovoids formed between PDMS and silica NPs (Figure 2a,b). The void formation led to new reflection interfaces (i.e., void/silica, void/PDMS, Figure 2c,d) and a dramatic increase (over 200 times) in the reflectance at the interface (0.014% to ≈3.05–3.45%) (see detailed calculation in the Supporting Information), and thus, a significant drop in transparency. Mechanical strain causes the thinning of the silica NP/PDMS composite film due to the positive Poisson's ratio of PDMS, 0.5. Since the top layer of silica NP/PDMS is much thinner than the bottom PDMS bulk layer, the thinning of the composite film should mainly occur in the bulk PDMS layer. Thus, the interplanar spacing (d_{planar}) of NP assembly should not change much with the strain, while location of voids should correlate to the silica NP positions (Figure 2c,d). The void arrangements formed locally should also be quasi-amorphous, analogous to the quasi-amorphous silica NP arrays, which were somewhat locked by the adjacent PDMS layer. Thus, the angle-independent structural color of the stretched films should be the result of the quasi-amorphous structures consisting of voids and silica NPs. As mentioned earlier, voids occurred locally at the high stress positions, and the local strain, obtained from the SEM images (Figure 2c), was on the order of 100% even at a relatively low global strain level. Based on the model in Figure 4a, the local volume filling fraction of voids (f_{void}) is calculated as ≈0.4, higher than that of air, f_{air} = 0.35,[29] of the sprayed quasi-amorphous array of NPs (see calculation in the Supporting Information). These results suggest that the local strain applied to the thin NP/PDMS layer is not equivalent to the global strain applied to the whole film; cracking/wrinkling and nanovoids occur to relax the local strain despite the continuing straining of the bulk PDMS layer. Therefore, the reflection peak position did not change with the increase of applied strain, while the peak intensity increased (Figure 3d) due to the increase in the number of voids. Likewise, blue-shift of the reflection peaks of stretched silica NP/PDMS film versus the as-prepared silica NP arrays can be explained by the decrease of d_{planar} and increase of f_{void} according to Equation S5 and S7 in the Supporting Information.

In addition to being a light blocking smart window (Video S1, Supporting Information) or a scattering surface for projectors, the composite film can also be used in display and security applications. Positive or negative letters can be embedded in the composite films by spray-coating of silica NPs on different masks, followed by mask removal and PDMS casting. As seen in Figure 4b and Video S2, Supporting Information, hidden letters "PENN" (negative) and "N" (positive) can be reversibly revealed upon stretching and releasing of the film.

In summary, we presented a smart optical window that could be reversibly switched from a highly transparent state (90% transmittance in the visible region) to opaqueness (30% transmittance) and display angle-independent reflective colors

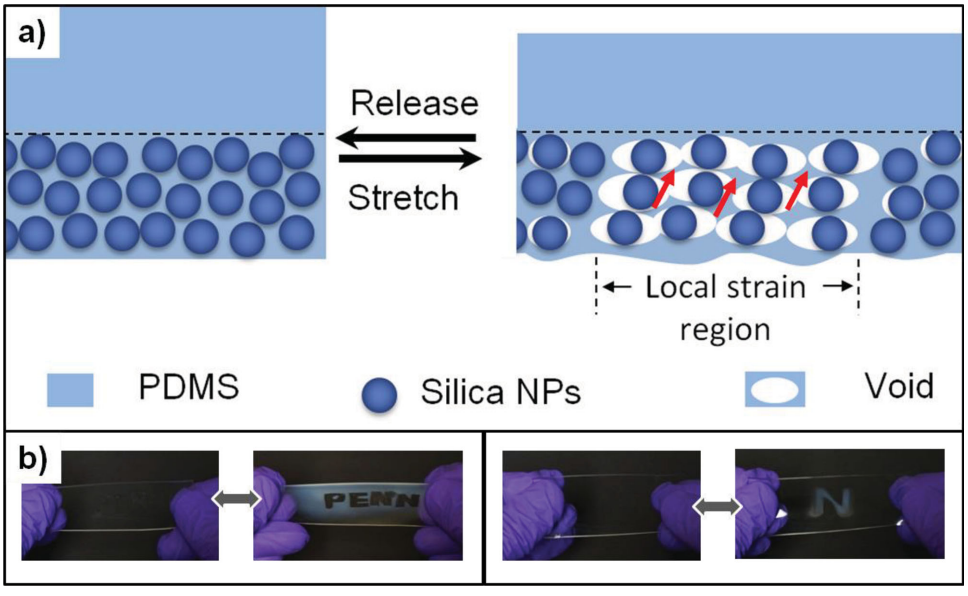

Figure 4. a) Schematic illustration of the void formation around the silica particles when stretched. The arrows indicate PDMS ligaments. b) Optical images showing reversible revealing and hiding of the letters patterned within the silica nanoparticle/PDMS film under mechanical stretching and releasing.

through mechanical stretching and release. The window was a bilayer elastomeric film consisting of a thin, hard layer of quasi-amorphous silica NP/PDMS and a thick, elastomeric layer of bulk PDMS. The displayed colors were found dependent only on the NP size, not the stretching strain, although they blue-shifted compared to the films prepared from NPs only. The dramatic change of optical responses is attributed to an increase of diffused light scattering and absorption resulting from the formation of microwrinkles and voids during stretching. The design of composite structures demonstrated here offers a facile and low-cost approach to dynamically and dramatically change optical properties. Compared to smart windows reported in the literature, ours have several unique characteristics, including: i) The initial state is truly transparent due to refractive index match between silica NPs and PDMS, whereas most smart windows are opaque or colored in the original state; ii) The change of transmittance in the vis–NIR region is very large, ≈60%; iii) The sprayed NPs are quasi-amorphous, therefore, much more robust against stretching in comparison to highly ordered colloidal crystals. They offer angle-independent color display upon stretching whereas most stretchable smart windows display angle-dependent colors; iv) The displayed color is independent of stretching strain, but dependent on NP size; v) The film is highly robust in repeated stretching and releasing (at least 1000 cycles) since the majority of the film under strain is the bulk PDMS layer. Although smart windows are demonstrated here for light transmission control, they can also be used in applications such as displays, camouflages, and security, as well as heat/solar gain control. The material design presented here offers new insights to dynamically and dramatically change physical properties. Further, the concept presented here can be applied to other functional material systems, such as liquid crystal elastomers and shape memory polymers, to design highly responsive, nano-/microstructured materials that are sensitive to heat, light, and moisture.

Experimental Section

Materials: Silica (SiO_2) NPs with diameter of 221, 258, and 306 nm were synthesized by the Stöber method.[9,10] The polydispersity of the SiO_2 NPs was less than 8%. Dow Corning Sylgard 184 silicone elastomer kit was used for preparing PDMS.

Fabrication of the Hybrid Window: SiO_2 NPs were dispersed into isopropyl alcohol (99.8%, Fisher Scientific, Inc.) at 10 wt% and ultrasonicated for 2 h (Branson Ultrasonic Cleaner, 2210) to prepare the spray solutions. The spray solution was loaded into an airbrush with nozzle size of 0.2 mm (Master Airbrush Model G44) and the operating pressure was 50 kPa. The solution was sprayed four times on the polystyrene (PS) Petri dish at a spray distance of 5 cm and a moving speed of ≈5 cm s^{-1}. Dow Corning Sylgard 184 silicone elastomer and curing agent were mixed at a weight ratio 10:1. After degassing, the PDMS precursor was cast on the sprayed PS Petri dish, and infiltrated into the voids of the silica NP film. The thickness of the PDMS film was controlled from 0.5 to 1 mm. The whole setup was then cured at 65 °C for 4 h. Finally, the hybrid film was carefully peeled from the PS Petri dish for stretching.

Fabrication of the Smart Window with Embedded Letters: A solid mask of "PENN" and a hollow mask of "N" were prepared from cut paper. The mask was placed on the Petri dish, followed by spray-coating of silica NPs. After removal of the mask, PDMS precursor was cast on the petri dishes following the same procedure to fabricate the hybrid window described above.

Characterization: SEM images were taken by FEI Quanta Field Emission Gun Environmental SEM in high vacuum mode at an acceleration voltage of 5 kV. The reflectance and scattering spectra at various strains and angles, and the time-dependent transmittance were collected from a USB4000 fiber optical spectrometer (Ocean Optics) combined with a custom-built stretcher and angle-resolved stage. Transmittance of the smart windows at various strains was measured using the Cary 5000 UV–vis–NIR spectrophotometer (Agilent Technologies) combined with a custom-built stretcher. Optical images were taken by optical microscopy (BX 61, Olympus) in reflection and transmission modes. In situ confocal microscopy was performed using a laser scanning confocal microscope (Thorlabs, Inc.) in reflection mode using a 635 nm laser source. Mechanical testing using this imaging modality was performed using a custom-built microtensile testing apparatus.

Supporting Information

Supporting Information is available from the Wiley Online Library or from the author.

Acknowledgements

D.G. and E.L. contributed equally to this work. This work is supported by the National Science Foundation (NSF)/EFRI-SEED grant (#EFRI-1038215). The Laboratory for Research on the Structure of Matter (LRSM), Penn NSF MRSEC (DMR-1120901), and Nanoscale Characterization Facility (NCF) are acknowledged for access to SEM. Dr. Milin Zhang (University of Pennsylvania) and Jenny Sabin (Cornell University) and her studio are acknowledged for helpful discussion and providing theoretical insights.

Received: January 19, 2015
Revised: February 9, 2015
Published online:

[1] M. G. Debije, *Adv. Funct. Mater.* **2010**, *20*, 1498.
[2] M. P. Gutierrez, L. P. Lee, *Science* **2013**, *341*, 247.
[3] M. P. Gutierrez, T. I. Zohdi, *Energy Buildings* **2014**, *71*, 95.
[4] D. Cupelli, F. Pasquale Nicoletta, S. Manfredi, M. Vivacqua, P. Formoso, G. De Filpo, G. Chidichimo, *Sol. Energy Mater. Sol. Cells* **2009**, *93*, 2008.
[5] C. Bechinger, S. Ferrere, A. Zaban, J. Sprague, B. A. Gregg, *Nature (London)* **1996**, *383*, 608.
[6] R. Baetens, B. P. Jelle, A. Gustavsen, *Sol. Energy Mater. Sol. Cells* **2010**, *94*, 87.
[7] J. D. Albert, B. Comiskey, J. M. Jacobson, L. Zhang, A. Loxley, R. Feeney, P. Drzaic, I. Morrison, *US Patent 6515649*, original assignee, E Ink Corporation, **2003**.
[8] C. Sheraw, L. Zhou, J. Huang, D. Gundlach, T. Jackson, M. Kane, I. Hill, M. Hammond, J. Campi, B. Greening, *Appl. Phys. Lett.* **2002**, *80*, 1088.
[9] J. L. West, in *Liquid-Crystalline Polymers*, ACS Symposium Series, Vol. 435, (Eds: R. A. Weiss, C. K. Ober), American Chemical Society, Washington, DC, **1990**, p. 475.
[10] D. Coates, *J. Mater. Chem.* **1995**, *5*, 2063.
[11] J. Wang, *US Patent 5270843*, Original Assignee, Jiansheng Wang, **1993**.
[12] P. S. Drzaic, *J. Appl. Phys.* **1986**, *60*, 2142.
[13] I. P. Parkin, T. D. Manning, *J. Chem. Ed.* **2006**, *83*, 393.
[14] C. M. Lampert, *Sol. Energy Mater.* **1984**, *11*, 1.

[15] S. Kinoshita, S. Yoshioka, *ChemPhysChem* **2005**, *6*, 1442.
[16] P. Vukusic, J. R. Sambles, *Nature (London)* **2003**, *424*, 852.
[17] M. Srinivasarao, *Chem. Rev.* **1999**, *99*, 1935.
[18] F. Liu, B. Q. Dong, X. H. Liu, Y. M. Zheng, J. Zi, *Opt. Express* **2009**, *17*, 16183.
[19] D. G. Stavenga, H. L. Leertouwer, N. J. Marshall, D. Osorio, *Proc. R. Soc. B: Biol. Sci.* **2010**.
[20] A. L. Holt, A. M. Sweeney, S. Johnsen, D. E. Morse, *J. R. Soc. Interface* **2011**, *8*, 1386.
[21] R. A. Potyrailo, H. Ghiradella, A. Vertiatchikh, K. Dovidenko, J. R. Cournoyer, E. Olson, *Nat. Photonics* **2007**, *1*, 123.
[22] S. Zylinski, S. Johnsen, *Curr. Biol.* **2011**, *21*, 1937.
[23] M. Izumi, A. M. Sweeney, D. DeMartini, J. C. Weaver, M. L. Powers, A. Tao, T. V. Silvas, R. M. Kramer, W. J. Crookes-Goodson, L. M. Mathger, R. R. Naik, R. T. Hanlon, D. E. Morse, *J. R. Soc. Interface* **2010**, *7*, 549.
[24] E. Lee, M. Zhang, Y. Cho, Y. Cui, J. Van der Spiegel, N. Engheta, S. Yang, *Adv. Mater.* **2014**, *26*, 4127.
[25] S. G. Lee, D. Y. Lee, H. S. Lim, D. H. Lee, S. Lee, K. Cho, *Adv. Mater.* **2010**, *22*, 5013.
[26] J. Li, J. M. Shim, J. Deng, J. T. B. Overvelde, X. L. Zhu, K. Bertoldi, S. Yang, *Soft Matter* **2012**, *8*, 10322.
[27] H. X. Xu, C. J. Yu, S. D. Wang, V. Malyarchuk, T. Xie, J. A. Rogers, *Adv. Funct. Mater.* **2013**, *23*, 3299.
[28] H. Fudouzi, T. Sawada, *Langmuir* **2005**, *22*, 1365.
[29] D. Ge, L. Yang, G. Wu, S. Yang, *Chem. Commun.* **2014**, *50*, 2469.
[30] K. Raman, T. R. S. Murthy, G. M. Hegde, *Phys. Proc.* **2011**, *19*, 146.
[31] I. H. Malitson, *J. Opt. Soc. Am.* **1965**, *55*, 1205.
[32] D. T. Ge, L. L. Yang, Y. Li, J. P. Zhao, X. Li, H. J. Zhao, *Synth. Met.* **2011**, *161*, 235.
[33] S. Yang, K. Khare, P.-C. Lin, *Adv. Funct. Mater.* **2010**, *20*, 2550.
[34] K. Chau, B. Millare, A. Lin, S. Upadhyayula, V. Nuñez, H. Xu, V. Vullev, *Microfluidics Nanofluidics* **2011**, *10*, 907.
[35] B. Millare, M. Thomas, A. Ferreira, H. Xu, M. Holesinger, V. I. Vullev, *Langmuir* **2008**, *24*, 13218.
[36] D. Ge, L. Yang, G. Wu, S. Yang, *J. Mater. Chem. C* **2014**, *2*, 4395.
[37] Y. Takeoka, S. Yoshioka, A. Takano, S. Arai, K. Nueangnoraj, H. Nishihara, M. Teshima, Y. Ohtsuka, T. Seki, *Angew. Chem. Int. Ed.* **2013**, *52*, 7261.